Spectroscopy 23 (2009) 11–28
DOI 10.3233/SPE-2009-0370
IOS Press

Discrimination of the binding mode of DNA ligands by single-photon timing

Luca Nardo [a,*], Maria Bondani [b] and Alessandra Andreoni [a]

[a] *Dipartimento di Fisica e Matematica and CNISM–CNR, Universita' degli Studi dell'Insubria, Como, Italy*

[b] *National Laboratory for Ultrafast and Ultraintense Optical Science – CNR–INFM, Como, Italy*

Abstract. We perform time-correlated single-photon counting measurements with 30-ps resolution of the fluorescence emitted by the donor fluorophores of donor–acceptor pairs covalently labeling DNA synthetic oligonucleotides by using a non-commercial single-photon avalanche diode. The measurements allow us to precisely assess the fluorescence resonant energy transfer efficiency of the pairs in solutions containing the oligonucleotides and DNA–ligands, for different ratios of the DNA base-pair to ligand concentrations. A quantitative evaluation of the deformations of DNA double strands following the ligand binding is obtained, as the transfer efficiency is a steep function of the donor-to-acceptor distance. The results lead to an easy and cheap method to discriminate between the binding modes of minor groove and base intercalating ligands.

Keywords: Binding-induced conformational transition, DNA base intercalator, DNA minor groove-binder, time-correlated single-photon counting, fluorescence resonance energy transfer

1. Introduction

The classic approach used to fight cancer, based on killing cancerous cells by employing radiations or chemotherapy, invariably kills the healthy cells too, often producing severe collateral effects. In the last thirty years researchers have been seeking for novel approaches to the design of anticancer drugs capable of acting on the cancerous cells in a selective way. A better understanding of how some small organic molecules (ligands) bind to DNA is required to further such selective approaches. In fact, the details of the binding are important to understand many biological processes that involve specific interactions of DNA structures with the substrate. For example, ligands might influence gene expression [1–4], and many of them show a variety of biological effects including antibiotic, antitrypanosomal and antiviral activity [1,5–7].

Many DNA ligands bind to DNA by base intercalation that is they interpose between adjacent Base Pairs (BP), inducing the unwinding of the double helices. Base Intercalators (BI) have been studied since the 1960s [8–10], and the main characteristics of this binding mode are well assessed. In particular, BIs typically display a binding length of 2 BP per ligand and thus no relevant sequence specificity. The unwinding of the helices induced by BIs causes an enhanced exposure of the bases to the solvent: thus, mutagenesis is dramatically increased [11–13]. For this reason, intercalators are dangerous carcinogens, even if their cytotoxicity has been widely exploited to devise antiviral drugs and in chemotherapy (see,

* Corresponding author: Luca Nardo, Dipartimento di Fisica e Matematica, Universita' degli Studi dell'Insubria and CNISM–CNR, Via Valleggio 11, 22100 Como, Italy. Tel.: +39 0312 386254; Fax: +39 0312 386119; E-mail: luca.nardo@uninsubria.it.

for instance, the use of antracyclines as anti-cancers [14]). However, due to the lack of sequence specificity, the chemotherapy of cancer based on such drugs is not tumor specific and particular care has to be used in establishing the correct dosage, finding a delicate equilibrium between maximization of anti-tumour effectiveness and minimization of both short- and long-term undesired toxic effects [15]. More recently, other ligands displaying a different binding mode, Minor Groove Binders (MGBs), have been recognized. Minor groove binding is a more complex binding mode than intercalation as MGBs covering a large range of binding lengths (from 3 to up to 10 BP per ligand) are known. The binding of an MGB to native DNA has no appreciable effect on the helices conformation. On the contrary, a stabilizing effect of MGBs on the helices with respect to the environmental action has been observed [16]. Most important, the great majority of MGBs display a very strong sequence specificity of the binding parameters. As a common feature of natural MGBs, the binding results to be much stronger in portions of the helices displaying sequences of at least 3–4 consecutive AT bases [17–21]. As a consequence, MGBs have demonstrated to be effective in inhibiting the sequence selective binding of various transcriptional factors to DNA. This may also result in either over-expression or repression of downstream genes [22–25]. Thus, ligands belonging to this second class offer the possibility of inducing targeted mutations to specific genes or genomic regions and appear promising for the development of tumor-cell selective drugs. Indeed, *in vivo* studies conducted on the MGB Pentamidine have revealed no mutagenic effect in nuclear DNA, and only very weak effects on mitochondrial DNA of yeast [1,26]. This result suggests that minor groove binding does not induce indiscriminate mutagenesis on nucleic acids.

Measuring the binding affinity of a ligand for DNA is nowadays fairly simple. Moreover, the availability of synthetic DNA of any desired sequence allows a straightforward comparison of the binding parameters of a ligand as a function of the base composition of the targeted DNA. On the contrary, determining the binding mode of a ligand is rather complicated. In spite of the profound differences occurring from BIs to MGBs as to the interaction with DNA and the therapeutic effects, the knowledge of the chemical structure of a ligand is not sufficient to forecast its way of binding. Even if most BIs are planar aromatic compounds, while the principal MGBs are unfused aromatic compounds, this rule is not always respected. Some ligands, such as 4′-6-diamidine-2-phenyl indole (DAPI) [27], can even bind to DNA in both ways, depending on the base sequence of the target. The only direct way of observing the specificities of the binding of a ligand is to perform X-ray diffraction experiments on crystals of the DNA–ligand complex [28–30]. Unfortunately, crystals of dimensions suitable for applications to diffraction methods are difficult to obtain. Moreover, the required technology is very expensive and the experimental results are often very difficult to interpret [31]. Even if molecular modeling can give some clue on determining the main features of a binding process, the results of simulations are affected by various approximations used during the docking process. Moreover, at present it is only possible to simulate the binding of ligands with very short DNA fragments (4–6 BP) [32]. As a consequence, the aim of the studies dealing with the computational approach is momentarily confined to test the ability of different modeling procedures to reproduce experimental data, while results which are not supported by experimental measurement of matching parameters are still not completely reliable. Thus, in their research of possible DNA targeting drugs, drug designers can only gain information on the binding mode of new natural and synthetic ligands by means of indirect, complicated and very expensive methods of investigation, such as viscosimetric titrations on native bacterial supercoiled circular DNA, footprinting inhibition or nuclear magnetic resonance [27,33].

In the present work, we show how an accurate detection of the deformations experienced by fragments of DNA suitably stained with fluorescent probes as a consequence of the binding of a ligand allows us to gain significant information regarding the ligand binding mode. We considered the DNA ligands DAPI,

quinacrine dihydrochloride (QUIN) and Hoechst 33258 (HOEC), whose binding mode has already been ascertained. We performed spectrophotometric titrations of the BI QUIN [34,35] and the MGB HOEC [36,37] with calf thymus (CT) DNA and spectrofluorimetric titrations of DAPI, which binds in the minor groove of AT-rich sequences but intercalates to GC-rich sequences [27,33,36,37], with the synthetic poly-nucleotides poly-d(AT) and poly-d(GC), to determine the specificities of their binding, and compared our results with those found in the literature. We then measured the fluorescence decay of a Donor fluorophore (D) attached to the 5′-end of double-stranded oligo-desoxyribonucleotides (Oligos), both in the presence and in the absence of a fluorescence Acceptor (A) at varying concentrations of each of the selected ligands. The measuring apparatus was a non-commercial time-correlated single-photon counting (TCSPC) system endowed with ∼30 ps resolution (full-width at half maximum duration of the pulse response) [38]. The variation in the fluorescence decay time of D due to A is proportional to the Fluorescence Resonance Energy Transfer (FRET) efficiency, thus to the D–A distance, so that the value of the decay time is itself a significant parameter to account for deformations of the helices following the binding. The ability to determine decay times with high precision and to directly reveal even decays as short as 30 ps, with no need of applying deconvolution techniques, besides allowing us to neatly assess the FRET efficiency between D and A, permitted to clearly distinguish the fraction of denatured helices in all the samples. As ligands that bind in the same way induce similar deformation and denaturation effects on the Oligos with which they interact, that are very different between MGBs and BIs, the results presented here encourage us to propose a protocol for easy and cheap discrimination between minor groove and intercalation binding modes.

2. Materials and methods

2.1. Chromophores

The free chromophores DAPI, QUIN and HOEC were supplied by Sigma-Aldrich, and were guaranteed to be at least 97% pure compounds. Stocks of about 1 mM concentration of the chromophores in bidistilled water were prepared. The fluorophores were further diluted in Phosphate Buffer Saline (PBS) at pH 7.58 and 100 mM ionic strength; 700 μM EDTA was added to PBS to prevent formation of dimers. The concentration values of the stocks in PBS were evaluated by absorption measurements with a spectrophotometer (Lambda 2 Perkin Elmer), by using the following values for the molar extinction coefficients: $\varepsilon_{\mathrm{QUIN}}$ (424 nm) = 9750 M^{-1} cm^{-1} [35], $\varepsilon_{\mathrm{DAPI}}$ (260 nm) = 30,000 M^{-1} cm^{-1} (specified by supplier), $\varepsilon_{\mathrm{HOEC}}$ (346 nm) = 46,000 M^{-1} cm^{-1} [39].

2.2. Polynucleotides

CT DNA, poly-d(AT) and poly-d(GC) were supplied by Sigma-Aldrich. Calf thymus DNA was in the form of sodium salt and was guaranteed to contain less than 5% protein impurities. The desiccated polynucleotides were diluted in PBS to ≈1 mM concentration and allowed to dissolve by keeping them overnight in the dark at the temperature of 4°C, gently stirring from time to time, before use. The concentration of the stock solutions was determined by absorption measurements using the value $\varepsilon_{\mathrm{DNA}}$ (260 nm) = 6600 M^{-1} cm^{-1} for the molar extinction coefficient.

2.3. Spectrophotometric and spectrofluorometric titrations

Quinacrine dihydrochloride: 30 ml of a 16.34 μM concentrated QUIN solution in PBS were prepared by dilution of the ≈1 mM concentrated stock in water. The ≈1 mM concentrated CT DNA solution was added with an appropriate amount of the same stock to get a final ligand concentration of 16.34 μM. At this QUIN-to-BP concentration ratio virtually all the ligand is bound to DNA. Two subsequent and independent measurements of the absorption spectrum of these solutions in the wavelength range from 300 to 650 nm were acquired. The ≈1 mM concentrated CT DNA, 16.34 μM concentrated QUIN solution was then progressively diluted with increasing amounts of the DNA-free, 16.34 μM concentrated QUIN solution, so as to obtain solutions of constant QUIN concentration and decreasing DNA concentration. Two absorption spectra were acquired for each of these solutions in the wavelength range from 300 to 650 nm. The mean absorbance value at the absorption peak of the ≈1 mM concentrated CT DNA, 16.34 μM concentrated QUIN solution, with an error given by the standard deviation, was chosen as the indicator of the fraction of bound ligand.

Hoechst 33258: the same procedure was followed to titrate CT DNA with HOEC, by working at 7.34 μM ligand concentration and acquiring the absorption spectra in the range from 300 to 650 nm.

4′-6-diamidine-2-phenyl indole: we prepared solutions similar to those prepared in the preceding cases, but instead of measuring the absorption, we decided to take advantage of the reported extraordinary fluorescence quantum yield enhancement displayed by DAPI when bound to DNA. Thus, for each solution, we acquired two fluorescence emission spectra in the wavelength range from 370 to 700 nm, by exciting the samples at 345 nm, with a spectrofluorometer (Fluorescence Master System PTI), and we chose the mean fluorescence value at the emission peak of the solution most concentrated in polynucleotide, with an error given by the standard deviation, as the indicator of the fraction of bound ligand. We worked at 6 μM DAPI concentration for the titration of poly-d(GC) and at 0.6 μM DAPI concentration for the titration of poly-d(AT), as the fluorescence enhancement consequent to the binding of DAPI to AT sequences is much more relevant.

2.4. Binding equilibrium data analysis

Binding isotherms were obtained from each titration by plotting the value of the relevant binding indicator, I (either absorbance or fluorescence intensity), versus the DNA concentration, P, expressed in BP concentration. The experimental binding isotherms were fitted to the independent site binding model equation [40]:

$$I = I_0 + \Delta I(nP) = I_0 + \frac{1}{2}\Delta I\left\{D + NP + \frac{1}{K_{\mathrm{Ass}}} - \left[\left(D + NP + \frac{1}{K_{\mathrm{Ass}}}\right)^2 - 4NPD\right]^{1/2}\right\}, \quad (1)$$

where D is the total ligand concentration (kept fixed to the experimental value during the fitting procedure), N is the number of binding sites per BP, K_{Ass} is the thermodynamic association constant, I_0 is the value taken by the binding indicator in the absence of DNA and is the difference between the value of the indicator at completely bound ligand and I_0.

The values obtained for I_0 and were used to calculate the values of the degree of saturation, n, of the binding sites (which is the number of bound ligand molecules per BP) from the equation

$$n = \frac{(I - I_0)D}{P\Delta I}. \quad (2)$$

Once n is known, the concentration of free ligand in solution, C, can be expressed as:

$$C = D - nP, \tag{3}$$

and the Scatchard plots (n/C versus n) can be obtained.

The Scatchard plots for HOEC and DAPI bound to poly-d(GC), which were linear, showing non-cooperative binding, could be fitted to the Scatchard equation [41]:

$$\frac{n}{C} = -K_{\text{Ass}} n + N K_{\text{Ass}}, \tag{4}$$

which is far more sensitive than Eq. (1) in assessing the N and K_{Ass} values.

In the case of QUIN, the Scatchard plot was concave upwards, indicating negatively cooperative binding. We thus derived the binding parameters from the McGhee and Von Hippel model, which only applies to ligands having binding length $L = 2$. In this condition, which is valid for the great majority of BIs, including QUIN, the following equation is satisfied [35]:

$$\frac{n}{C - nP} = \mathrm{K}_{\text{Ass}} \left[\frac{(2\omega - 1)(1 - 2n) + n - R}{2(\omega - 1)} \right] \left[\frac{1 - 3n + R}{2(1 - 2n)} \right], \tag{5}$$

where $R = [(1 - 3n)^2 + 4\omega n(1 - 2n)]^{1/2}$ and ω is a cooperativity parameter which equals 1 for no cooperative effect, is less than 1 for anti-cooperative binding and greater than 1 for positive cooperativity.

In the case of DAPI bound to poly-d(AT), the Scatchard plot was concave downwards, indicating positively cooperative binding. As for most MGBs, for DAPI we have $L \neq 2$, and the more general, although empiric, Hill model [42] must be applied. The model allows to find K_{Ass} and the so called Hill constant, α_{Hill}, which measures the degree of cooperativity and can take values between 1 (no cooperative effects) and L (in case of perfect positive cooperativity, that is when the binding of a single ligand molecule induces immediate binding of other ligand molecules to the complete saturation of all the binding sites). The fitting equation is:

$$\ln(C) = -\frac{1}{\alpha_{\text{Hill}}} \ln\left(\frac{N}{n}\right) - \ln K_{\text{Ass}}. \tag{6}$$

Linearity of the plot of $\ln(C)$ versus $\ln(N/n)$ is forecast by Eq. (6). The N value has to be inferred from the analysis of the Scatchard plot. Anyway, if the guess on the N value overestimates the real value, the Hill plot will be concave upwards, while if it underestimates the real value the Hill plot will be concave downwards.

In all the cases, the fitting procedures were implemented with a commercial software featuring Levenberg–Marquardt algorithm (Origin 7.0 by OriginLab). It should be noted that, upon deriving a Scatchard plot from a titration dataset, the data-points corresponding to negligible amounts of either bound or free ligand are usually rejected as the error on the n/C value is expected to increase very steeply if either n or C gets close to zero. However, we included and fitted data well beyond the normally used range, which corresponds to $0.2D \leqslant C \leqslant 0.8D$.

2.5. Oligos

Labeled Oligos purified by double HPLC procedure were purchased from Sigma-Genosys. We used the single labeled Oligos:

D-5′(AT)3′: TAMRA-TAAATATAATATTTATTAAATATAA,
D-5′(GC)3′: TAMRA-GCGCCCCCCCCCCGCCCCCCCCCG,

and the dual labeled Oligos:

D-5′(AT)3′-A: TAMRA-TAAATATAATATTTATTAAATATAA-BHQ2,
D-5′(GC)3′-A: TAMRA-GCGCCCCCCCCCCGCCCCCCCCCG-BHQ2,

where the D-Chromophore bound at the 5′ end was 5-carboxytetramethylrhodamine (TAMRA), and the A bound at the 3′ end was the Sigma-Aldrich patented, non-emitting quencher Black Hole Quencher 2 (BHQ2), which is a polyaromathic azo compound that is capable of efficient quenching of many of the most widely used chromophores and shows no detectable fluorescence.

The reported sequences were designed to show no tendency to formation of primer dimers and very weak tendency to formation of secondary structures. Unlabeled Oligos of complementary sequences, purified by DST and double RP1 procedures, were also purchased from Sigma-Genosys. The desiccated Oligos were dissolved in PBS at 100 μM concentration and stored at -20°C until use. Double stranded Oligos were obtained by mixing equal concentrations (50 μM) of labeled single stranded sequences and complementary fragments, heating up to 98°C and leaving the samples cool very slowly to room temperature. This procedure assured denaturation of secondary structures of the single strands, and allowed us to obtain a hybridized fraction of the samples always greater than 0.9. The annealed stocks were also kept frozen at -20°C until use.

2.6. Single photon timing setup

The timing setup is fully described elsewhere [38]. However, at variance with [38], in the present work the TAMRA fluorescence was excited by the second harmonic (532 nm, TEM_{00} beam) of a SESAM mode locked Nd:VAN laser delivering pulses at 113 MHz repetition rate (GE-100-1064-VAN Time Bandwidth Products, Zurich-CH). As in [38], the beam exciting the sample was focused on it by a lens of 150 mm focal length. The sample was held in a 1 cm thick, 1 cm wide, 4 cm high quartz cuvette, mounted on a 3D micro-movable support. Fluorescence at 90 deg to the excitation beam was collected from a wide acceptance angle by means of a reversed 40× microscope objective, which was 3D micro-movable and tiltable to center the focal spot onto the 50 μm diameter sensitive area of the detector, which was a single photon avalanche diode (SPAD) endowed with quantum efficiency at the fluorescence peak wavelength (577 nm) and $<$100 Hz dark counts (PDM50 Micro Photon Devices, Bolzano, Italy). The SPAD was mounted on a third 3D micro-positioning system. The electric signals were treated as in [38]. The typical response to the excitation pulse had $<$35 ps full-width at half-maximum duration.

2.7. Preparation of the samples for fluorescence decay measurements

The solutions for lifetime determination were prepared by dilution of the stocks to TAMRA concentration values below 0.35 μM, so as to get an absorbance value of less than 0.05 at the fluorescence peak wavelength, in order to prevent concentration-quenching. The concentrations of the different compounds were inferred by weighting with a balance with 100 μg sensitivity. To avoid photodegradation

of the samples and possible effects on the fluorescence decays due to dilution of D's, titrations were performed by preparing distinct solutions with the same Oligo concentration value and varying ligand concentration values.

2.8. Fluorescence decay data acquisition and processing

All decay patterns were collected in strict single photon regime (detected photon rate <100 kHz to have a ratio $P(>1)/P(1) < 0.01$, where $P(1)$ is the probability of detecting one fluorescence photon per laser pulse and $P(>1)$ is the probability of detecting more than one photon) by suitably attenuating the excitation beam with neutral density filters. Collection of excitation stray light by the microscope objective was prevented by putting a long-wavelength pass filter with cut at 600 nm between cuvette and objective. Sample, microscope objective and SPAD were kept in a black box even if measurements were taken in the dark, to avoid detection of light diffused from the laser beam.

The decay patterns as measured by the TCSPC system were fitted either with single or double exponential decay functions above a constant background, i.e. $f(t) = B + \sum_{i=1}^{2} A_i \exp(-t/\tau_i)$ by minimizing the chi-squared value through a Levenberg–Marquardt algorithm, using Origin 7.0. The amplitudes, A_i, were calculated at the peak channel of the experimental curves. Three decay patterns were acquired for each sample. As the final values of τ_i and A_i of each decay component we assumed the means of the values obtained by the three fits, with the statistical errors given by the standard deviations.

In this work we make use of the <35 ps temporal resolution to correctly evaluate both the A_i of a fast decay component without need of deconvolving the pulse response and the small differences between relatively long τ_i values observed upon changing the ligand-to-BP ratio. The former feature allows us to evaluate the amount of denaturation, the latter to detect tiny DNA deformations. In Fig. 1 we show decay patterns that are critical as they are well fitted by single-exponential functions with very similar and relatively long τ_i values. The figure also shows the corresponding fitting curves $f(t)$ and the plots of the residuals.

3. Results

We first present our binding studies on the selected ligands. The binding isotherm obtained for the spectrophotometric titration of CT DNA with QUIN is displayed in Fig. 1(a), in which the absorbance at 434.4 nm is plotted versus P. In the figure inset the absorption spectra of the 16.34 μM concentrated free QUIN solution (grey line) and of the ≈1 mM DNA, 16.34 μM QUIN concentrated solution (black line) are reported: the bound ligand displays substantial hypochromicity (the molar extinction coefficient value at the absorption peak is lower than for the free ligand) and a 10 nm red shift. The corresponding Scatchard plot was concave upwards (data not shown), and the N value derived by fitting the binding isotherm to Eq. (1) (solid line in Fig. 2(a)) was $N = (0.20 \pm 0.02) \ll 1/L = 0.5$, revealing the anti-cooperative nature of the binding. The McGhee and Von Hippel model has been used to derive the binding parameters. The relevant plot is reported in Fig. 2(b). The data are well fitted by Eq. (5), with $K_{\mathrm{Ass,QUIN}} = ((2 \pm 1) \times 10^5)\ \mathrm{M}^{-1}$ and $\omega = 0.14 \pm 0.03$, in good agreement with Wilson and coworkers [35].

The binding isotherm obtained for the spectrophotometric titration of CT DNA with HOEC is displayed in Fig. 3(a), in which the absorbance at 352.8 nm is plotted versus P. In the figure inset the absorption spectra of the 7.34 μM concentrated free HOEC solution (grey line) and of the ≈1 mM DNA,

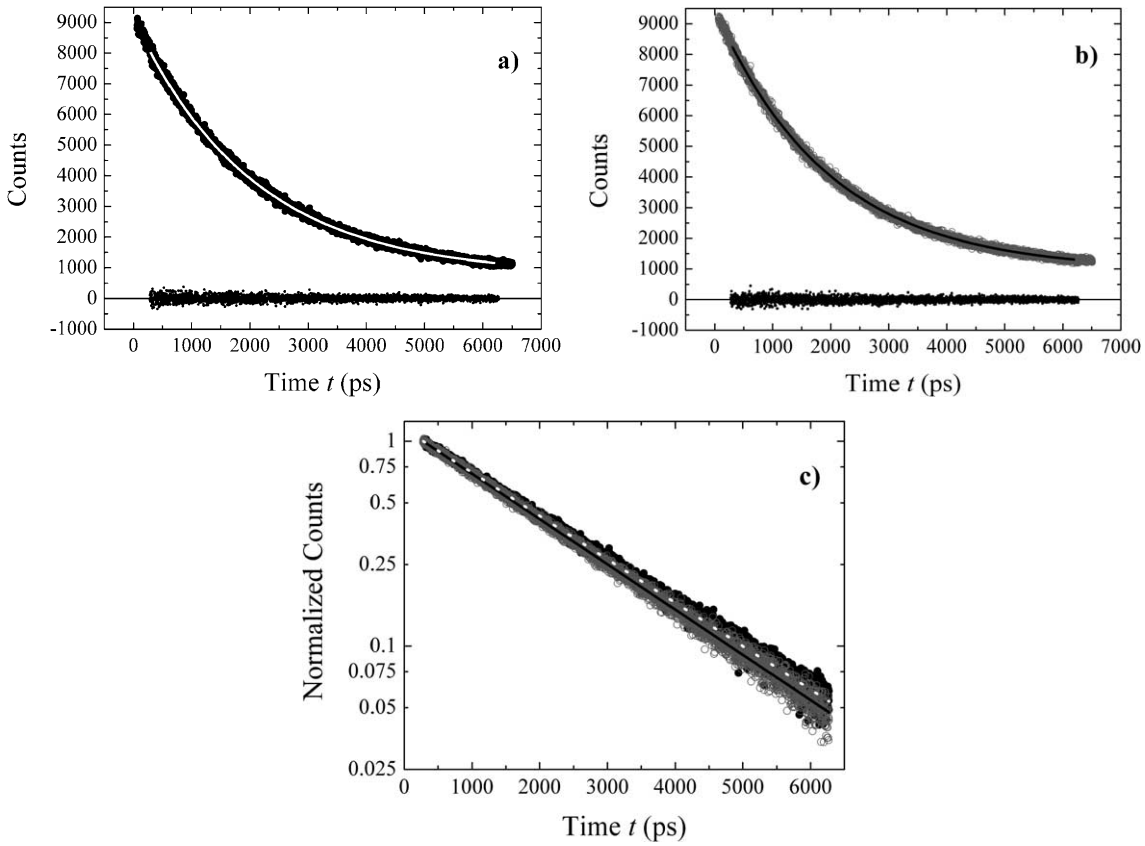

Fig. 1. Fluorescence decay patterns of TAMRA-(AT)-BHQ2 titrated with DAPI at DAPI-to-BP ratios of 1.9 in (a) and 16.23 in (b), corresponding best fitting curves and residuals. The fitting parameters to the single exponential decay $f(t) = B + A_1 \exp(-t/\tau_1)$ are: in (a) $B = (752.87 \pm 5.84)$ counts, $A_1 = (9900.35 \pm 10.07)$ counts, $\tau_1 = (2048.93 \pm 5.19)$ ps; in (b) $B = (938.19 \pm 5.48)$ counts, $A_1 = (10163.47 \pm 10.63)$ counts, $\tau_1 = (1965.67 \pm 4.77)$ ps. In (c) the two decays normalized to A_1 after subtraction of background B are plotted on a logarithmic scale.

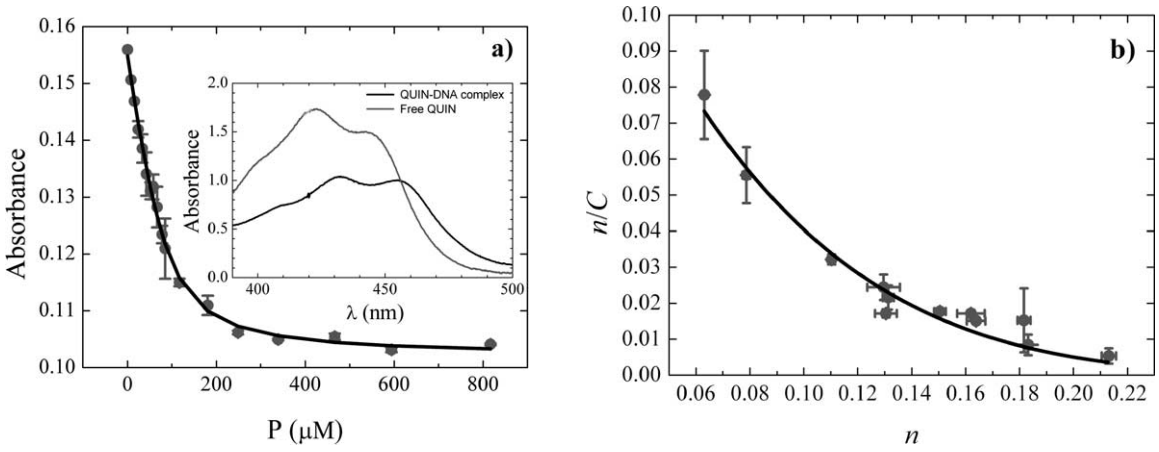

Fig. 2. Binding isotherm obtained from the spectrophotometric titration of CT DNA with QUIN: (a) absorbance at 434.4 nm versus DNA concentration. In the inset the absorption spectra of bound (black) and free (grey) QUIN, as a function of the wavelength, λ. (b) Scatchard plot (circles), fitted to the McGhee and Von Hippel equation (solid line).

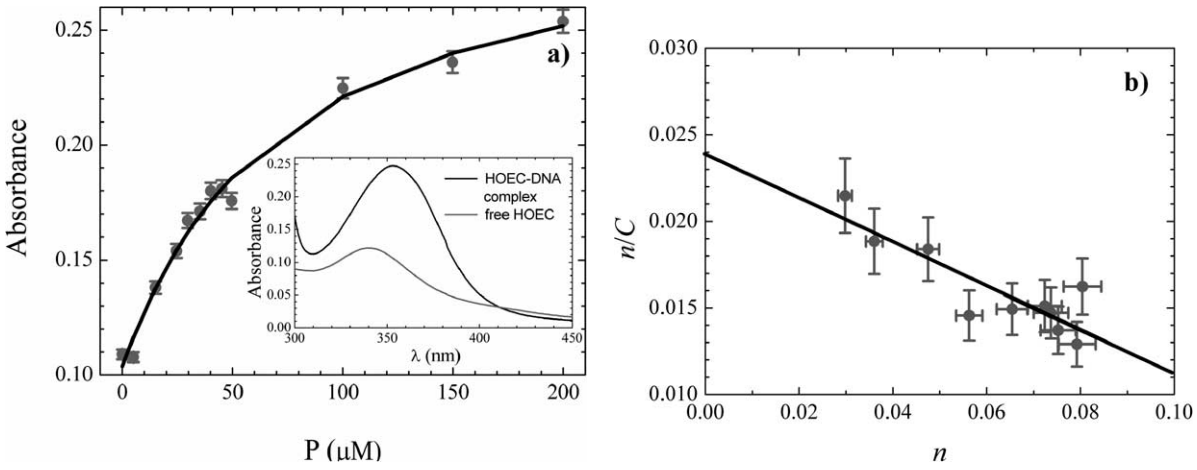

Fig. 3. Binding isotherm obtained from the spectrophotometric titration of CT DNA with HOEC: (a) absorbance at 352.8 nm versus DNA concentration. In the inset the absorption spectra of bound (black) and free (grey) HOEC. (b) Scatchard plot (circles) fitted to the non-cooperative Scatchard model (solid line).

7.34 μM HOEC concentrated solution (black line) are reported: the bound ligand displays substantial hyperchromicity (the molar extinction coefficient value at the absorption peak is higher than for the free ligand) and a 12 nm red shift. The corresponding Scatchard plot is linear (see Fig. 3(b)), indicating non-cooperative binding. The data are well fitted by Eq. (4), with $K_{\mathrm{Ass,HOEC}} = ((1.3 \pm 0.3) \times 10^5)\ \mathrm{M}^{-1}$ and $N = 0.19 \pm 0.05$, corresponding to $L = 5.3 \pm 1.4$.

The binding isotherm obtained for the spectrofluorometric titration of poly-d(AT) with DAPI is displayed in Fig. 4(a), in which the fluorescence intensity at 456 nm is plotted versus P. In the figure inset the fluorescence spectra of the 0.6 μM concentrated free DAPI solution (grey line) and of the ≈1 mM DNA, 0.6 μM DAPI concentrated solution (black line) are reported: the bound ligand is ≈80 times more fluorescent than the free ligand, and the emission peak is 4 nm blue-shifted. The corresponding Scatchard plot, reported in Fig. 4(b), is concave downwards, revealing the cooperative nature of the binding. The fit of the experimental titration data to Eq. (1) (solid line in Fig. 4(a)) gave $N = 0.16 \pm 0.01$. Interpolation of the Scatchard plot data with a parabola (grey solid line in the inset in Fig. 4(b)) gave the guess value $N \cong 0.13$, while linear interpolation (black solid line in the inset in Fig. 4(b)) of the five data points on the descent of the Scatchard plot (indicated by arrows in the same figure) gave the guess value $N \cong 0.18$. The McGhee and Von Hippel model could thus not be used to derive the binding parameters. Hill plots were derived at varying the N value in the interval $0.13 \leqslant N \leqslant 0.18$; the best linearity was obtained for $N = 0.16$, corresponding to $L \cong 6$: the relevant plot is reported in Fig. 4(b). The data are well fitted by Eq. (6), with $K_{\mathrm{Ass,DAPI-AT}} = ((4.9 \pm 0.4) \times 10^6)\ \mathrm{M}^{-1}$ and $\alpha_{\mathrm{Hill}} = 2.4 \pm 0.2$. Significant cooperativity of the binding and $K_{\mathrm{Ass,DAPI-AT}} \approx 10^7\ \mathrm{M}^{-1}$, with $L \cong 4$, were reported by Wilson and coworkers [27,33], and substantially agree with our findings.

The binding isotherm obtained for the spectrofluorometric titration of poly-d(GC) with DAPI is displayed in Fig. 5(a), in which the fluorescence intensity at 478 nm is plotted versus P. In the figure inset the emission spectra of the 6 μM concentrated free DAPI solution (black line) and of the ≈1 mM DNA, 6 μM DAPI concentrated solution (grey line) are reported. To allow direct comparison with the corresponding spectra obtained in the poly-d(AT) titration, the present data have been normalized to account for the difference in ligand concentration. The bound ligand is ≈20 times more fluorescent than the free ligand, and the emission peak is 18 nm red-shifted. The corresponding Scatchard plot is linear (see

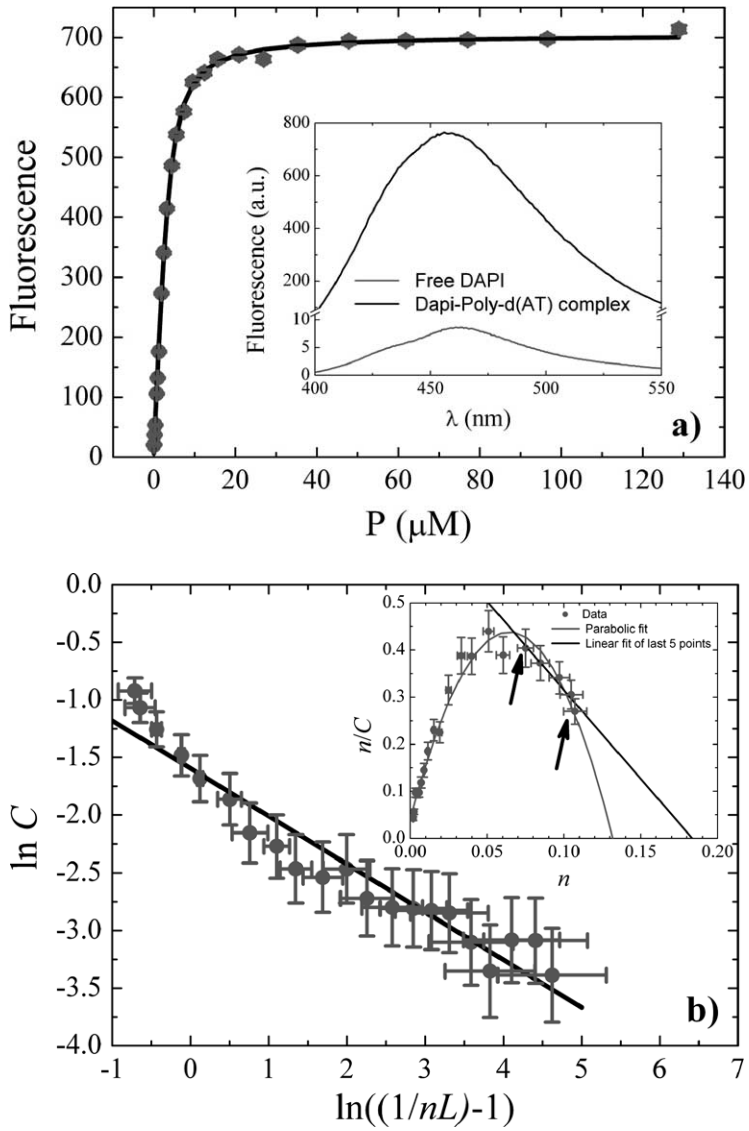

Fig. 4. Binding isotherm obtained from the spectrophotometric titration of poly-d(AT) with DAPI: (a) fluorescence at 456 nm versus DNA concentration. In the inset the fluorescent emission spectra of bound (black) and free (grey) DAPI. (b) Hill plot (circles) fitted to the Hill equation (solid line). In the inset: the Scatchard plot (dots) is concave downwards, indicating cooperative binding. The N value is in the range 0.13–0.18, as can be inferred by linear (black line) and parabolic (grey line) extrapolation of the intercept with the x-axis.

Fig. 5(b)), and the N value derived by fitting the binding isotherm to Eq. (1) (solid line in Fig. 5(a)) was $N = 0.52 \pm 0.03$, as expected for a BI, indicating non-cooperative binding. The Scatchard plot is well fitted by Eq. (4), with $K_{\mathrm{Ass,DAPI-GC}} = ((6.4 \pm 0.4) \times 10^5)\ \mathrm{M}^{-1}$ and $N = 0.53 \pm 0.04$, corresponding to $L \cong 2$. These parameters are in good agreement with those reported by Wilson et al. [27].

We now present the time resolved fluorescence data we acquired on the TAMRA-labeled Oligos. We initially measured fluorescence decay patterns of the TAMRA bound to both the single-stranded and the annealed dual-labeled Oligos, and to the annealed single-labeled Oligos. The measured time constants τ_i

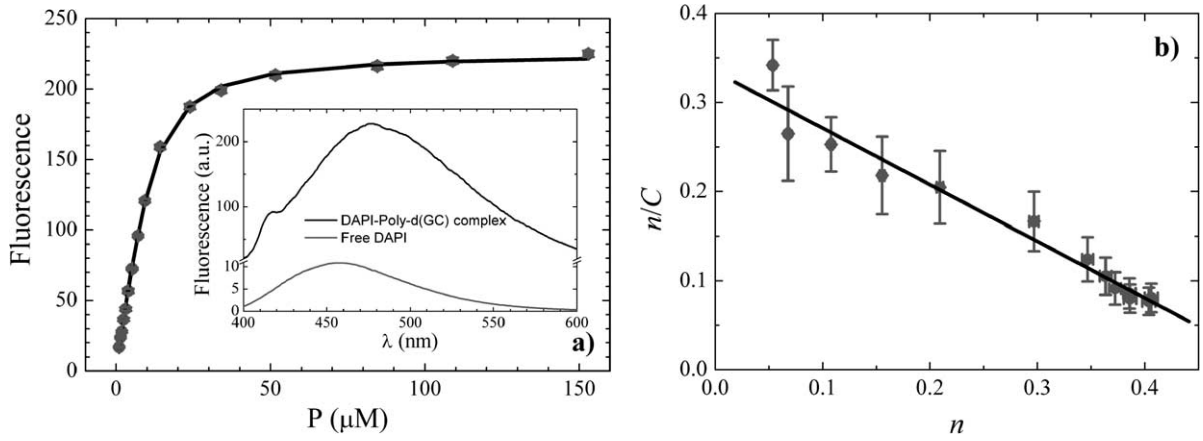

Fig. 5. Binding isotherm obtained from the spectrofluorometric titration of poly-d(GC) with DAPI: (a) fluorescence at 478 nm versus DNA concentration. In the inset the fluorescent emission spectra of bound (black) and free (grey) DAPI. (b) Scatchard plot (circles) fitted to the non-cooperative Scatchard model (solid line).

Table 1

Time constants, τ_i (ps), and relative amplitudes, f_i, where $i = L, S$ (see text), as derived from the fits of the fluorescence decay patterns of TAMRA bound to the dual-labeled Oligos either annealed or single-stranded and to single-labeled annealed Oligos

Oligos	τ_L (ps)	f_L	τ_S (ps)	f_S
TAMRA-(AT)				
Annealed	3046 ± 14	1	–	–
TAMRA-(AT)-BHQ2				
Annealed	2163 ± 5	1	42 ± 5	$\approx$0
Single stranded	$\approx$2500	$\approx$0	42 ± 5	1
TAMRA-(GC)				
Annealed	2657 ± 15	1	–	–
TAMRA-(GC)-BHQ2				
Annealed	1754 ± 3	1	31 ± 4	$\approx$0
Single stranded	$\approx$2100	$\approx$0	31 ± 4	1

Note: $f_{L,S} \approx 0$ stands for $f_{L,S} < 0.05$.

are collected in Table 1, where $i = 1 \equiv L$ stands for long and $i = 2 \equiv S$ for short decay time, along with their relative amplitudes:

$$f_i = \frac{A_i}{\sum_{j=1}^{2} A_j}. \tag{7}$$

Notably, TAMRA attached to single-labeled Oligos of both sequences has single exponential decays, while TAMRA attached to both single-stranded and annealed dual-labeled Oligos has double exponential decay. As the long decay time is dominant for the annealed samples, we can attribute τ_L to the fluorescence of the fraction of D labeling the annealed strands. Interestingly, the τ_L values measured for these samples are significantly lower than those measured for the corresponding single-labeled Oligos. This evidence indicates that the TAMRA fluorescence is efficiently quenched by BHQ2 when the Oligos assume the double-helical structure. Similarly, as the short decay time is dominant in the decay of the

single-stranded samples, we attribute to the fluorescence of the fraction of D's labeling the single strands. The observation that $\tau_S \ll \tau_L$ can be explained if the much shorter persistence length (bases) of the Oligos in the single-stranded structure is taken into account. The flexibility of the chain allows the collapse of the single-stranded Oligos into random coil, in which the hydrophobic bases are shielded from the solvent while the hydrophilic sugar–phosphate backbone is exposed. The $5'$ and $3'$ ends of the Oligos are near in these compact structures, thus very efficient quenching of TAMRA fluorescence by BHQ2 occurs. In the very rigid annealed Oligos, whose persistence length is $\geqslant$50 base pairs (BP), the D and the A are spaced by the whole Oligo length, and quenching, although still occurring, is slower. Traces of long-lived components in the single-stranded samples may be due to the presence of Oligos labeled with inactive quencher, which have already been detected in similar samples by single molecule fluorescence techniques [44–46]. In fact, τ_L is longer for these samples than for the corresponding dual-labeled annealed samples, and very similar to that measured for the single-labeled ones. The observation of a residual short-lived coiled fraction even in double-helical samples may be due to incomplete annealing.

We then performed titrations of TAMRA-(AT)-BHQ2 dual labeled annealed Oligos with HOEC, an MGB and DAPI, that binds in the minor groove of AT-rich sequences but intercalates to GC sequences, whose minor groove is shallower and less profound [27]. The value of the short-decay time, when this component had detectable amplitude, did not significantly change both following titration with DAPI and HOEC. The short-lived fraction also kept constant at varying the ligand concentration, showing no denaturation as a consequence of binding. In Fig. 6(a) (full dots) the long-decay time for DAPI titration is reported, as a function of the ratio of the concentration of ligand molecules to the concentration of DNA–BP, in the following simply referred to as ligand-to-BP ratio. The data show that a fast increase in lifetime sets in at minimal DAPI-to-BP ratio, followed by a decrease down to an almost constant value, which is lower than that measured in the absence of DAPI, at DAPI-to-BP ratios exceeding $\sim$0.35. The corresponding long lifetime data for titration with HOEC (full dots in Fig. 6(b)) show a similar behavior at high ligand-to-BP ratios (lifetimes are somewhat shorter than those measured in the absence of HOEC), but the increase of at low ligand-to-BP ratios is lacking.

We also measured the fluorescence decays of TAMRA labeling the BHQ2-free AT sequence at DAPI and HOEC concentrations similar to those used in the titrations. We observed no changes in the fluorescence decay with changing the ligand-to-BP ratio. The obtained values are plotted as empty circles in Fig. 6(a) and (b), respectively. We can thus conclude that exclusively the quenching action of BHQ2 is responsible for the lifetime changes observed for titration of the dual-labeled Oligos. Indeed, any direct

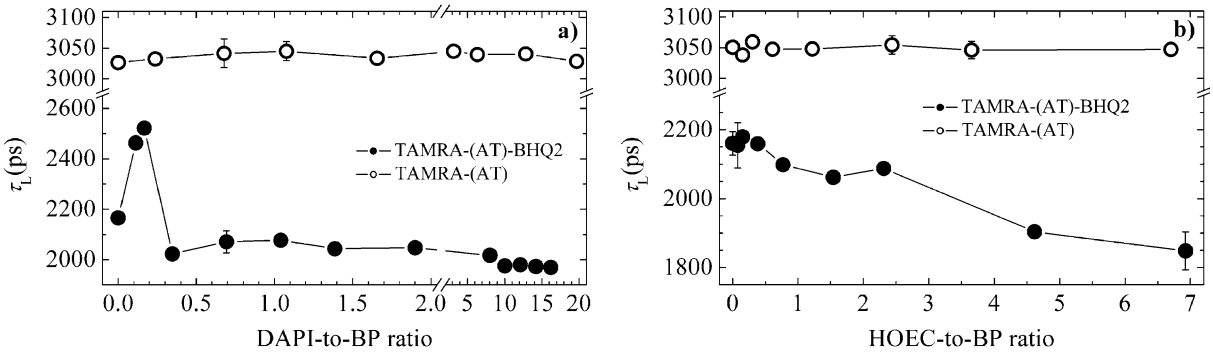

Fig. 6. Full dots: long-decay time for titrations of TAMRA-(AT)-BHQ2 with (a) DAPI, and (b) HOEC as a function of ligand-to-BP ratio. Empty circles: same data for titrations of BHQ2-free TAMRA-(AT).

TAMRA-ligand interaction leading to dynamic quenching of the TAMRA fluorescence would be evidenced also in the absence of BHQ2. Significant spectral shifts of the TAMRA emission band, which would result in changes in the BHQ2 FRET efficiency, would also correspond to variations. Thus they can be ruled out.

A very different behavior is exhibited by TAMRA-(GC)-BHQ2 intercalated with DAPI. Once again, the presence of DAPI in solution does not affect the TAMRA fluorescence decay in BHQ-free TAMRA-labeled GC sequences (see empty circles in Fig. 7(a)). The long decay-time of TAMRA-(GC)-BHQ2 (full dots in the figure) very rapidly increases for DAPI-to-BP ratios of up to about 6:1. Then it keeps approximately constant. Similar features are displayed for TAMRA-(AT)-BHQ2 titrated with the BI QUIN, as shown in Fig. 7(b).

As another common feature, the short lifetime fraction f_S grows as a function of the ligand-to-BP ratio in both the titration of TAMRA-(GC)-BHQ2 with DAPI (triangles in Fig. 8) and of TAMRA-(AT)-BHQ2 with QUIN (squares in Fig. 8). The sigmoidal trend of f_S is the signal of a strong tendency to denaturation of the double-helical structure as an effect of binding.

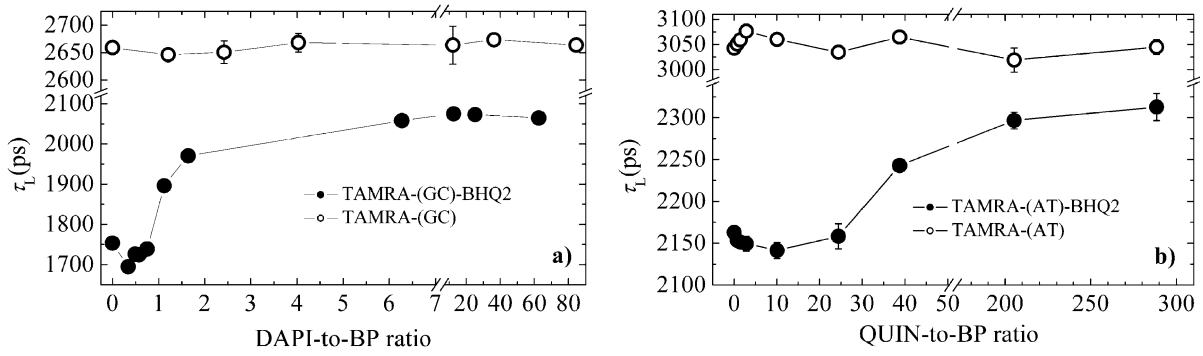

Fig. 7. Full dots: long-decay time for titrations of (a) TAMRA-(GC)-BHQ2 with DAPI, and (b) TAMRA-(AT)-BHQ2 with QUIN as a function of the ligand-to-BP ratio. Empty circles: same data for titrations of BHQ2-free TAMRA-(GC) and TAMRA-(AT).

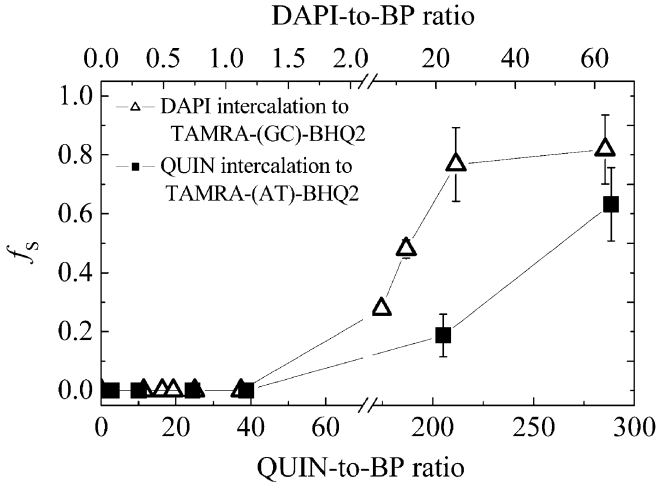

Fig. 8. Fraction of Oligos in the single helical coiled state as a function of the ligand-to-BP ratio for intercalation of DAPI to TAMRA-(GC)-BHQ2 (triangles) and of QUIN to TAMRA-(AT)-BHQ2 (squares).

4. Discussion

Our data definitely show the capability of our TCSPC system of monitoring structural and conformational changes induced in double stranded Oligos by the binding of a number of ligands. A very neat qualitative distinction between the conformational changes induced by minor groove binding and those induced by intercalation is evidenced. First of all, the binding of both MGBs does not produce any changes in either τ_S or f_S. The τ_S value also remains constant upon titration with the BIs, but f_S increases by adding such ligands with a sigmoidal trend. We interpret this evidence as denaturation of the double-helical structure due to BIs but not to MGBs binding. The second difference is that, by adding large amounts of ligand, τ_L asymptotically decreases for both the MGBs and increases for both BIs. The increase in τ_L accompanying the intercalation of a ligand (see Fig. 7) is to be expected. It is due to the unwinding of the double strands, which brings TAMRA to a greater distance from BHQ2 with respect to the relaxed unperturbed double-helical structure. Denaturation (see Fig. 8) can also be explained as a consequence of unwinding, as exposure of the bases to the solvent has the effect of cutting hydrogen bonds.

On the contrary, we did not expect a shortening of the TAMRA decay time in the case of minor groove binding (see Fig. 6). It might be caused by bending of the annealed Oligos caused by steric interaction ingenerated by the insertion of the MGBs in the minor groove. Indeed, it is well known that, in a perfect B-stranded DNA double helix, the minor groove makes a complete turn around the axis of the helix every 10 BPs. Our Oligos are made of 25 BPs. If we consider them to be in a perfect B-strand conformation, as the MGBs can be hosted only in the minor (and not in the major) groove, and the minor groove does not turn around the helical axis of an Oligo an integer number of times, but only makes 2.5 turns, there results to be a side of the helix on which less MGB molecules are bound, and the opposite side bearing an excess of MGB molecules. Steric interactions are likely to happen by which the minor groove is enlarged to host the ligand molecule. In excess of MGB (saturated binding sites) such widening is equally distributed along the whole minor groove. As the minor groove runs preferentially on one side of the helix, this widening causes bending on the side of the helix where the minor groove has not completed its third turn. As a consequence of bending, TAMRA is brought nearer to BHQ2, and quenching is enhanced. The titration data (see Figs 3 and 4 for HOEC and DAPI, respectively) allow us to explain the saturation of the lifetime decrease at low ligand-to-BP ratios, observed for both ligands. It is due to the saturation of all the available binding sites, that are very few, as a large number of BP are engaged in the binding of a single ligand ($L \cong 5$ for HOEC and $L \cong 6$ for DAPI , corresponding to only $\approx$5 binding sites per Oligo for HOEC, $\approx$4 for DAPI). Such saturation occurs at very low ligand-to-BP ratios as the binding affinity is very strong (see the determined K_{Ass} values) and, in case of DAPI, the binding is strongly cooperative (see Fig. 4(b) inset). The increase in lifetime of the long-lived component of TAMRA obtained at low DAPI-to-BP ratios (Fig. 6(a)) is possibly the signature of a peculiar and not previously observed conformational change, resulting in a considerable increase in the length of the double-stranded fragments. A similar behavior has been reported for other MGBs, such as Netropsin and Distamycin, binding to Calf Thymus and Chicken Erythrocyte DNA [47]. In both cases, similarly to what we observed for DAPI, the helices recover their original length by increasing the MGB concentration. Moreover, an allosteric model has been proposed to account for the cooperativity of the binding of DAPI to poly d(A-T) [27], depicting a conformational transition, involving the widening of minor grooves following the binding of the first DAPI molecules.

Another interesting outcome of our data is a direct confirmation of the assertion that intercalation is a substantially non-specific binding mode both with respect to the structural and chemical peculiar-

ities of the BI and with respect to the base sequence of the titrated DNA. To show this, we need to calculate, for the titrations of TAMRA-(GC)-BHQ2 with DAPI and TAMRA-(AT)-BHQ2 with QUIN, the degree of saturation n of the binding sites at each ligand-to-BP ratio. This is possible by using Eq. (3) to eliminate the unknown variable C in Eqs (4) and (5), provided that reliable values are available for the binding parameters of DAPI to GC sequences and of QUIN to AT sequences. Such values were derived by means of the titrations of poly-d(GC) and CT DNA, respectively, presented in the first part of this work. Equations (4) and (5) can thus be solved to calculate the n value corresponding to each D. Our experimental technique allows us to determine the FRET efficiency, E, of BHQ2 on TAMRA since:

$$E = 1 - \frac{\tau_{D+A}}{\tau_D}, \tag{8}$$

where τ_{D+A} and τ_D are the excited-state lifetimes of TAMRA in the presence and in the absence of BHQ2, respectively. As E depends on the D–A distance, R, through the relation [48]:

$$E = \frac{R_0^6}{R_0^6 + R^6}, \tag{9}$$

where R_0 is the Förster radius, that is the D–A distance at which $E = 1/2$, equating Eqs (8) and (9) yields:

$$\frac{R}{R_0} = \left(\frac{\tau_D}{\tau_{D+A}} - 1\right)^{-1/6} \tag{10}$$

and makes it possible to determine R in units of R_0. Note that, if the fluorescence decay times are precisely measured, the method can detect very tiny variations in the D–A distance. Note also that, as R_0 depends on the relative orientation of the TAMRA and BHQ2 transition dipole moments [48], in principle R_0 can vary during titration if, for example, addition of the ligand induces changes in the solvent viscosity. Similarly, changes in the medium refractive index are reflected in changes to the R_0 value. Anyway, at such low concentrations as those used in this work, ligands can hardly significantly affect the buffer properties. Assuming that R_0 does not vary significantly upon addition of either DAPI or QUIN, and neglecting the contribution of the short tethers, we can thus take R/R_0 as a measure of the DNA unwinding induced by the BIs.

If we plot the R/R_0 values calculated from the experimental decay time data versus n for DAPI bound to GC sequences (full dots in Fig. 9) and QUIN bound to AT sequences (empty circles in Fig. 9), we obtain an amazingly similar unwinding effect for both ligands. This result definitely supports the fact that we are measuring ligand-induced changes in the length of the Oligos rather than changes in the D–A distance or in the D spectral properties due to ligand interactions with either D or A. On the contrary, the minor groove binding of HOEC and DAPI to AT sequences cause different conformational changes, as it is apparent by comparison of the full dotted patterns of Fig. 6(a) and (b). This is probably because the different chemical structures of different MGBs, together with the possibility of having a quite variable number of ligand molecules hosted in each minor groove, have a relevant and quite unpredictable effect on the peculiarities of the steric interactions leading to deformation of the groove.

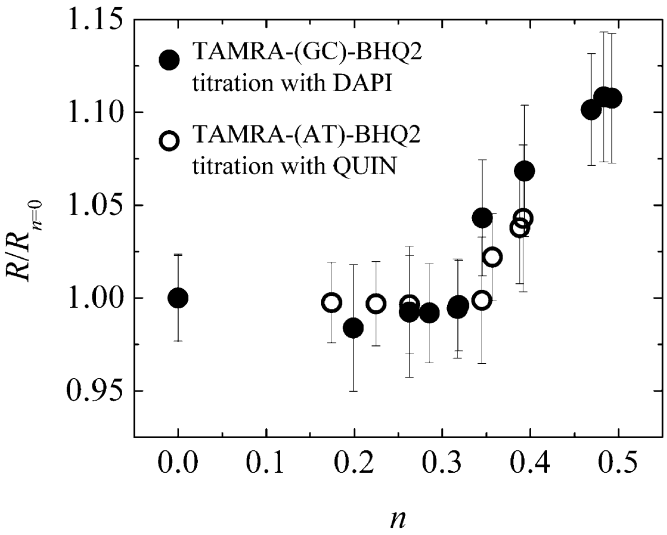

Fig. 9. Donor–acceptor distance (in units of R_0) as a function of the degree of saturation of the binding sites, n, for intercalation of DAPI to TAMRA-(GC)-BHQ2 (full dots) and of QUIN to TAMRA-(AT)-BHQ2 (empty circles).

5. Conclusions

We have developed a protocol allowing an easy discrimination between DNA–ligands binding in the minor groove and DNA–ligands binding by base intercalation, which we consider to be a helpful tool in selecting potential DNA-targeting drugs. The protocol is based on the capability of obtaining a quantitative indication of the deformations experienced by double-stranded synthetic Oligos as a consequence of the binding of a ligand. This is achieved by means of TCSPC measurements, with 30-ps time resolution, of the fluorescence emitted by the D fluorophore of a D–A pair covalently labeling the Oligos. The binding of BIs induces (i) the unwinding of the double-helices with consequent increase of the D–A distance and of the D fluorescence lifetime and (ii) the denaturation of the double-helical structure with consequent appearance of a short-living transient in the D fluorescence decay. These features are not observed for MGBs, for which the fast decay component does not appear, indicating no denaturation, and the D fluorescence lifetime tends to shorten at increasing ligand-to-BP ratio.

Our analysis has also allowed detecting a peculiar allosteric transition in the binding of the ligand DAPI to the minor groove of Oligos with AT sequences. Finally, our procedure can be used to study the binding of a ligand to different base sequences so as to assess the binding sequence specificity, as demonstrated in the case of DAPI.

We finally point out that we actually revealed ligand-induced changes in the length/conformation of the Oligos rather than changes in D–A distances or D spectral properties due to ligand interactions with the donor and the acceptor. If these interactions were relevant the coincidence of the two graphs in Fig. 9 would not be found.

Acknowledgements

The authors are grateful to S. Cova, M. Ghioni and I. Rech (Politecnico di Milano, Italy) for the continuing collaboration with the SPAD's. The technical assistance with the electronics offered by G. Zambra

(Como) is also acknowledged. This work was supported by the Italian Ministry for Instruction, University and Research through the MIUR-PRIN 2005027857 grant.

References

[1] P.R. Turner and W.A. Denny, The mutagenic properties of DNA minor groove binding ligands, *Mutation Research* **355** (1995), 141–169, and references therein.
[2] J.M. Gottersfeld, J.M. Belitsky, C. Melander, P.B. Dervan and K. Luger, Blocking transcription through a Nucleosome with synthetic DNA ligands, *J. Mol. Biol.* **321** (2002), 249–263.
[3] M.R. Mattern, S.M. Mong, H.F. Bartus, C.K. Mirabelli, S.T. Crooke and R.K. Johnson, Relationship between the intracellular effects of comptothecin and inhibition of topoisomerase I in cultured L1210 cells, *Cancer Research* **47** (1987), 1793–1798.
[4] J.S. Adhikari, D. Khaitan, M.B. Arya and B.S. Dwarakamath, Heterogeneity in the radiosensitizing effects of the DNA ligand Hoechst 33342 in human tumor cell lines, *J. Cancer Res. Therap.* **1** (2005), 151–161.
[5] S.A. Latt, Optical studies of metaphase chromosome organization, *Ann. Rev. Biophys. Bioeng.* **5** (1976), 1–37.
[6] E.F. Gale, E. Cundiffe, P.E. Reynolds, M.H. Richmond and M.J. Waring, *The Molecular Basis of Antibiotic Action*, Wiley, London, 1981.
[7] C. Zimmer and U. Wahnert, Nonintercalating DNA-binding ligands: specificity of the interaction and their use as tools in biophysical, biomedical and biological investigations of the genetic material, *Prog. Biophys. Mol. Biol.* **47** (1986), 31–112.
[8] L.S. Lerman, Structural considerations in the interaction of DNA and acridines, *J. Mol. Biol.* **3** (1961), 18–30.
[9] L.S. Lerman, The structure of the DNA–acridine complex, *Proc. Natl. Acad. Sci. USA* **49** (1963), 94–102.
[10] J.D. McGhee and P.H. Von Hippel, Theoretical aspects of DNA–protein interactions: Cooperative and non-cooperative binding of large ligands to a one-dimensional homogeneous lattice, *J. Mol. Biol.* **86** (1974), 469–489.
[11] L. Strekowsky, Molecular basis for the enhancement and inhibition of bleomycin-madiated degradation of DNA by DNA-binding compounds, *Adv. Detail. React. Mech.* **2** (1992), 61–109.
[12] R.D. Sneyder and M.S. Diehl, The bleomycin amplification assay in V79 cells predicts frameshift mutagenicity of intercalative agents, *Mutagenesis* **15** (2000), 203–205.
[13] R.S. Iyer, B.F. Coles, K.D. Raney, R. Their, F.P. Guengerich and T. M. Harris, DNA adduction by the potent carcinogen Aflatoxin B-1 – Mechanistic studies, *J. Am. Chem. Soc.* **116** (1994), 1603–1609.
[14] V. Malatesta and A. Andreoni, Dynamics of anthracyclines/DNA interaction: a laser time-resolved fluorescence study, *Photochem. Photobiol.* **48** (1988), 409–415.
[15] J.F. Boivin, Second cancers and other late side effects of cancer treatment, *Cancer* **65** (1990), 770–775.
[16] A.N. Sinyakov, S.G. Lokhov, I.V. Kutyavin, H.B. Gamper and R.B. Meyer Jr., Exceptional and selective stabilization of A-T rich DNA–DNA duplexes by N-Methylpyrrole Carboxamide peptides conjugated to oligodeoxynucleotides, *J. Am. Chem. Soc.* **117** (1995), 4995–4996.
[17] Y. Bathyni, K.E. Rao, R.G. Shea and J.W. Lown, Molecular recognition between ligands and nucleic acids: novel pyridine and benzoxazole-containing agents related to Hoechst 33258 that exhibit altered DNA sequence specificity deduced from footprinting analysis and spectroscopic studies, *Chem. Res. Toxicol.* **3** (1990), 268–280.
[18] A.L. Drobisshev, A.S. Zasedatelev, G.M. Yershov and A.D. Mirzabekov, Massive parallel analysis of DNA–Hoechst 33258 binding specificity with a generic oligodeoxyribonucleotide microchip, *Nucleic Acid Res.* **27** (1999), 4100–4105.
[19] S.Y. Breusegem, R.M. Clegg and F.G. Loontiens, Base-sequence specificity of Hoechst 33258 to DNA and DAPI binding to five $(A/T)_4$ DNA sites with kinetic evidence for more than one high-affinity Hoechst 33258-AATT complex, *J. Mol. Biol.* **315** (2002), 1049–1061.
[20] T. Stokke and H.B. Steen, Multiple binding modes for Hoechst 33258 to DNA, *J. Histochem. Cytochem.* **33** (1985), 333–338.
[21] P.G. Baraldi, M.A. Tabrini, D. Preti, F. Fruttarolo, B. Avitabile, A. Bovero, G. Pavani, M. Nunez Carretero and R. Romagnoli, DNA minor-groove binders. Design, synthesis and biological evaluation of ligands structurally related to CC-1065, distamycin and antramycin, *Pure Appl. Chem.* **75** (2003), 187–194.
[22] A.K. Basu, C.J. Hanrahan, S.A. Malia, S. Kumar, R. Bizanek and M. Tomasz, Effect of site specifically located mitomycin C-DNA adducts on *in-vitro* DNA synthesis by DNA polymerases, *Biochemistry* **32** (1993), 4708–4718.
[23] T.A. Beerman, M.M. Mc Hugh, R. Sigmund, J.W. Lown, K.E. Rao and Y. Bathini, Effects of analogs of the DNA minor groove binder Hoechst 33258 on Topoisomerase II and I mediated activities, *Biochem. Biophys. Acta* **1131** (1992), 53–61.
[24] M. Broggini and M. D'Incalci, Modulation of transcription factor–DNA interactions by anticancer drugs, *Anticancer Drug Design* **9** (1994), 373–387.
[25] J.P. Bruzik, D.T. Auble and P.L. de Haseth, Specific activation of transcription initiation by the sequence-specific DNA-binding agents distamycin A and netropsin, *Biochemistry* **26** (1987), 950–956.

[26] W.A. Denny, New directions in the design of anticancer drugs, *Drug Des. Deliv.* **3** (1988), 99–124.
[27] W.D. Wilson, F.A. Tanious, H.J. Barton, R.L. Jones, K. Fox, R.L. Wydra and L. Strekowski, DNA sequence dependent binding modes of 4′-6-diamidino-2-phenylindole (DAPI), *Biochemistry* **29** (1990), 8452–8461.
[28] M.L. Kopka, P. Pjura, C. Yoon, D. Goodsell and R.E. Dickerson, The binding of netropsin to double-helical B-DNA of sequence C-G-C-G-A-A-T-T-BrC-G-C-G: single crystal x-ray structure analysis, in: *Structure and Motion: Membranes, Nucleic Acids and Proteins*, E. Clementi, G. Corougin, M.H. Sarma and R. Sarma, eds, Adenine Press, New York, 1985, pp. 461–483.
[29] M.L. Kopka, C. Yoon, D. Goodsell, P. Pjura and R.E. Dickerson, The molecular origin of DNA–drug specificity in netropsin and distamycin, *Proc. Natl. Acad. Sci. USA* **82** (1985), 1376–1380.
[30] M.L. Kopka, C. Yoon, D. Goodsell, P. Pjura and R.E. Dickerson, Binding of an antitumor drug to DNA, netropsin and C-G-C-G-A-A-T-T-BrC-G-C-G, *J. Mol. Biol.* **183** (1985), 553–563.
[31] G.S. Couch, D.K. Hendrix and T.E. Ferrin, Nucleic acid visualization with UCSF Chimera, *Nucleic Acids Res.* **34** (2006), e29, and references therein.
[32] L.F. Pineda De Castro and M. Zacharias, DAPI binding to the DNA minor groove: a continuum solvent analysis, *J. Mol. Recogn.* **15** (2002), 209–220, and references therein.
[33] F.A. Tanious, J.M. Veal, H. Buczak, L.S. Ratmeyer and W.D. Wilson, DAPI (4′-6-diamidino-2-phenylindole) binds differently to DNA and RNA: minor groove binding at AT sites and intercalation at AU sites, *Biochemistry* **31** (1992), 3103–3112.
[34] S. Jockusch, A.A. Marti, N.J. Turro, Z. Li, J. Ju, N. Stevens and D. L. Akins, Spectroscopic investigation of a FRET molecular beacon containing two fluorophores for probing DNA/RNA sequences, *Photochem. Photobiol. Sci.* **5** (2006), 493–498.
[35] W.D. Wilson and I.G. Lopp, Analysis of cooperativity and ion effects in the interaction of quinacrine with DNA, *Biopolymers* **18** (1979), 3025–3041, and references therein.
[36] N. Morii, G. Kido, T. Konakahara and H. Morii, Orientation of dye molecules in DNA-based films with chain alignment and judgment of their DNA-binding modes, *J. Phys. Chem. B* **109** (2005), 15636–15644.
[37] M. Rueda, F.J. Luque and M. Orozco, Nature of minor-groove binders-DNA complexes in the gas phase, *J. Am. Chem. Soc.* **127** (2005), 11690–11698.
[38] L. Nardo, R. Paderno, A. Andreoni, M. Màsson, T. Haukvik and H.H. Tønnesen, Role of H-bond formation in the photoreactivity of curcumin, *Spectroscopy* **22** (2008), 187–198.
[39] H. Du, R.A. Fuh, J. Li, L.A. Corkan and J.S. Lindsey, PhotochemCAD: a computer-aided design and research tool in photochemistry, *Photochem. Photobiol.* **68** (1998), 141–142.
[40] A. Abbotto, G. Baldini, L. Baverina, G. Chirico, M. Collini, L. D'Alfonso, A. Diaspro, R. Magrassi, L. Nardo and G.A. Pagani, Dimethyl-pepep: a DNA probe in two photon excitation cellular imaging, *Biophys. Chem.* **114** (2005), 35–41.
[41] G. Scatchard, The attraction of proteins for small molecules and ions, *Ann. N.Y. Acad. Sci.* **51** (1949), 660–672.
[42] A.V. Hill, The possible effects of the aggregation of the molecules of hemoglobin on its dissociation curves, *J. Physiol.* **40** (1910), IV–VII.
[43] A.L. Lacaita, M. Ghioni and S. Cova, Double epitaxy improves single-photon avalanche diode performance, *Electron. Lett.* **25** (1989), 841–843.
[44] A.A. Deniz, M. Dahan, J.R. Grunwell, T. Ha, A.E. Faulhaber, D.S. Chemla, S. Weiss and P.G. Schultz, Single-pair fluorescence resonance energy transfer on freely diffusing molecules: observation of Förster distance dependence and subpopulation, *Proc. Natl. Acad. Sci. USA* **96** (1999), 3670–3675.
[45] A.A. Deniz, T.A. Laurence, M. Dahan, D.S. Chemla, P.G. Schultz and S. Weiss, Ratiometric single-molecule studies of freely diffusing biomolecules, *Annu. Rev. Phys. Chem.* **52** (2001), 233–253.
[46] M.C. Murphy, I. Rasnik, W. Cheng, T.M. Lohman and T. Ha, Probing single-stranded DNA conformational flexibility using fluorescence spectroscopy, *Biophys. J.* **86** (2004), 2530–2537.
[47] N. Dattagupta, M. Hogan and D.M. Crothers, Interaction of netropsin and distamycin with deoxyribonucleic acid: electric dichroism study, *Biochemistry* **19** (1980), 5998–6005.
[48] T. Förster, Experimentelle und theoretisch untersuching des zwischenmolekularen übergangs von elektronenanregungsenergie, *Z. Naturf.* **4a** (1949), 321–327.